Batteries & Supercaps

Research Article
doi.org/10.1002/batt.202300075

Chemistry Europe
European Chemical Societies Publishing

www.batteries-supercaps.org

High-Voltage Operation of All-Oxide Solid-State Sodium Batteries Using NASICON-Related Materials

Dai Kutsuzawa*[a] and Takeshi Kobayashi[a]

All-oxide solid-state sodium batteries (AOSSSBs), which are composed of oxide electrolytes and oxide active materials with sodium-ion carriers, have attracted attention because of their high safety and material abundance. However, the operating voltage of AOSSSBs is inevitably low because the number of active materials available for use in AOSSSBs is restricted by undesirable reactions at electrolyte/electrode interfaces during high-temperature fabrication. Herein, we fabricate AOSSSBs using a Na superionic conductor-type solid electrolyte $Na_3Zr_2(SiO_4)_2(PO_4)$ (NZSP), a Na superionic conductor-type negative active material $NaTi_2(PO_4)_3$, and a mixed-phosphate cathode active material $Na_4Ni_3(PO_4)_2(P_2O_7)$ by a $Na_2B_4O_7 \cdot 10H_2O$-assisted low-temperature fabrication technique. The obtained $NaTi_2(PO_4)_3$/NZSP/$Na_4Ni_3(PO_4)_2(P_2O_7)$ batteries exhibit an average discharge voltage of 3.1 V, which is the highest voltage ever reported in AOSSSBs. In addition, $Na_2B_4O_7 \cdot 10H_2O$-containing NZSP electrolytes show a wider electrochemical window in comparison with the pristine NZSP, enabling the batteries to endure a wide voltage operation (a capacity retention of 71% after 10 cycles of charge/discharge in 0–5.1 V).

Introduction

All-oxide solid-state sodium batteries (AOSSSBs), which are composed of oxide active materials and oxide electrolytes and are charged/discharged by sodium-ion transfer from a positive/negative electrode to the counter (negative/positive) electrode, have been promoted as highly safe and sustainable next-generation batteries. Although lithium-ion batteries are commonly used in electric vehicles and energy storage systems nowadays, there are some severe risks in the batteries from the hazardous nature of flammable liquid electrolytes[1] and from the shortage and the associated price increase of lithium.[2] Recently, research into solid-state batteries has been widely pursued because of the high degree of safety afforded by the presence of non-flammable solid electrolytes only. Among the many types of solid-state batteries, such as those based on sulfides or polymers, oxide-based batteries tend to show higher safety because of their high thermal and chemical stability.[3] The use of sodium as a carrier ion, rather than lithium, is beneficial, because sodium is a more abundant and less expensive element.[4]

Although several works on AOSSSBs have been reported recently, the operating voltages of AOSSSBs in these studies have been limited to narrow ranges. For example, the most common AOSSSBs, which consist of $Na_3V_2(PO_4)_3$ negative and positive electrodes and $Na_3Zr_2(SiO_4)_2(PO_4)$-related solid electrolytes, showed average discharge voltages of 1.3–1.7 V with operating voltage ranges of 0–2.5 V.[5–8] In other studies, $Na_3V_2(PO_4)_3$/$Na_3Zr_2(SiO_4)_2(PO_4)$/$Na_4Co_3(PO_4)_2(P_2O_7)$ batteries[9] and $Na_2Ti_3O_7$/β''-Al_2O_3/P_2-$Na_{2/3}Fe_{1/2}Mn_{1/2}O_2$ batteries[10] exhibited average discharge voltages of 1.8 V and 2.1 V with operating voltage ranges of 0.5–3.9 V and 1.0–4.0 V, respectively, which were undesirably low in comparison with the voltages expected from half-cells using liquid electrolytes. An all-NASICON battery, $Na_3V_2(PO_4)_3$/$Na_5YSi_4O_{12}$/$Na_3V_2(PO_4)_2O_2F$, was demonstrated to show an operating voltage of 1.0–3.0 V, although a $Na_5YSi_4O_{12}$/polymer composite electrolyte was used in the battery to overcome poor oxide/oxide contact.[11]

One reason for the low operating voltages of AOSSSBs is the limited number of active materials available for use in AOSSSBs, because most active materials are unstable against high-temperature battery fabrication. Generally, high-temperature sintering is required to form oxide/oxide rigid interfaces, which ensure conduction paths throughout AOSSSBs. However, such a high-temperature process often causes undesirable reactions between the active materials and the solid electrolytes, leading to the degradation of AOSSSBs. For the sake of avoiding degradation, $Na_3V_2(PO_4)_3$/$Na_{3+x}Zr_2(SiO_4)_{2+x}(PO_4)_{1-x}$/$Na_3V_2(PO_4)_3$ batteries, for instance, were successfully fabricated at relatively low temperature[6,8] or within short sintering time,[7] although the operating voltage of the batteries was intrinsically low ($<$1.8 V). Kobayashi et al. developed a multi-step fabrication process to utilize a high-potential cathode active material, $Na_4Co_3(PO_4)_2(P_2O_7)$, without its decomposition into $NaCoPO_4$ at 600 °C, but a relatively high operating temperature (200 °C) was required to overcome the inevitably high resistance of electrolyte/electrolyte interfaces.[9] Thus, a novel fabrication technique is necessary to broaden the range of material choices available for AOSSSBs.

In the present study, we fabricated AOSSSBs with a Na superionic conductor (NASICON)-type solid electrolyte $Na_3Zr_2(SiO_4)_2(PO_4)$ (NZSP), a NASICON-type anode active material $NaTi_2(PO4)_3$ (NTP), and a mixed phosphate-type cathode active material $Na_4Ni_3(PO_4)_2(P_2O_7)$ (NNPP), namely NTP/NZSP/NNPP batteries, by using a flux-assisted low-temperature fabrication technique.[5] In this method, premixing of a

[a] Dr. D. Kutsuzawa, Dr. T. Kobayashi
Central Research Institute of Electric Power Industry
240-0196 Yokosuka (Japan)
E-mail: kutsuzawa3866@criepi.denken.or.jp

Supporting information for this article is available on the WWW under https://doi.org/10.1002/batt.202300075

Research Article
doi.org/10.1002/batt.202300075
Chemistry Europe
European Chemical Societies Publishing

$Na_2B_4O_7 \cdot 10H_2O$ (NBO) sintering aid into the NZSP electrolyte facilitates the batteries to be densified at the relatively low temperature of 600 °C. The redox potential of NNPP is 4.3–5.1 V vs. Na/Na^+ (between $Na_4Ni_3(PO_4)_2(P_2O_7)$ and $NaNi_3(PO_4)_2(P_2O_7)$),[12] whereas the redox potential of NTP is 2.1 V vs. Na/Na^+ (between $NaTi_2(PO_4)_3$ and $Na_3Ti_2(PO_4)_3$) and 0.4 V vs. Na/Na^+ (between $Na_3Ti_2(PO_4)_3$ and $Na_4Ti_2(PO_4)_3$),[13] which should result in a high operating voltage of 2.2–4.7 V for the NTP/NZSP/NNPP batteries. The mechanism of the charge/discharge profiles of the batteries was elucidated by measuring the battery voltage-dependent change of crystal structures in the batteries. In addition, the stability of the batteries against high-voltage charge/discharge cycles was investigated.

Results and Discussion

The NTP/NZSP/NNPP batteries were successfully fabricated at 600 °C by mixing the NBO sintering aid into both the electrolyte layer and the electrode layers. Figure 1 shows X-ray diffraction (XRD) patterns of the NNPP positive electrode and the NTP negative electrode in the NTP/NZSP/NNPP batteries. When the batteries were fabricated at 750 °C without the NBO, both electrodes contained strong peaks that were derived from unidentified phases and weak peaks derived from active materials, which means that the active materials were decomposed during the batteries fabrication. However, when the batteries were fabricated at 600 °C with the NBO, the peaks from the unidentified phases were not observed, suggesting that the undesirable decomposition of the active materials during fabrication was suppressed by the lower-temperature fabrication technique. Cross-sectional secondary electron microscopic images revealed that the electrode layers in the batteries fabricated at 600 °C were composed of smaller size of grains in comparison to those fabricated at 750 °C (Supporting Information, Figure S1), implying that grain growth was inhibited by the lower-temperature fabrication. In the NTP electrode, subtle $Na_4TiO(PO_4)_2$ impurity peaks were still observed, which indicates that the NTP active materials were slightly decomposed even at 600 °C.

The highest voltage ever reported in AOSSSBs was achieved during the first discharge process in the obtained NTP/NZSP/NNPP batteries. The NTP/NZSP/NNPP batteries exhibited a discharge capacity of 56 mAh g^{-1} (based on the loading mass of the NNPP active material), a coulombic efficiency of 65%, and an average discharge voltage of 3.1 V in the first cycle (Figure 2a). This capacity was quite similar to the capacity of an NNPP half-cell using a liquid electrolyte (57 mAh g^{-1}, Supporting Information Figure S2a) but lower than those of carbon-coated NNPP half-cells in previous works, 63 mAh g^{-1}[12] and 74 mAh g^{-1},[14] whereas the coulombic efficiency of the NTP/NZSP/NNPP batteries was relatively high compared with those of the carbon-coated NNPP half-cells, 48%[12] and 55%.[14] One possible reason for this relatively low capacity is the presence of electrically isolated NNPP active materials, because, in this study, we adopted uncoated NNPP active materials, for which the electronic conductivity is assumed to be significantly low

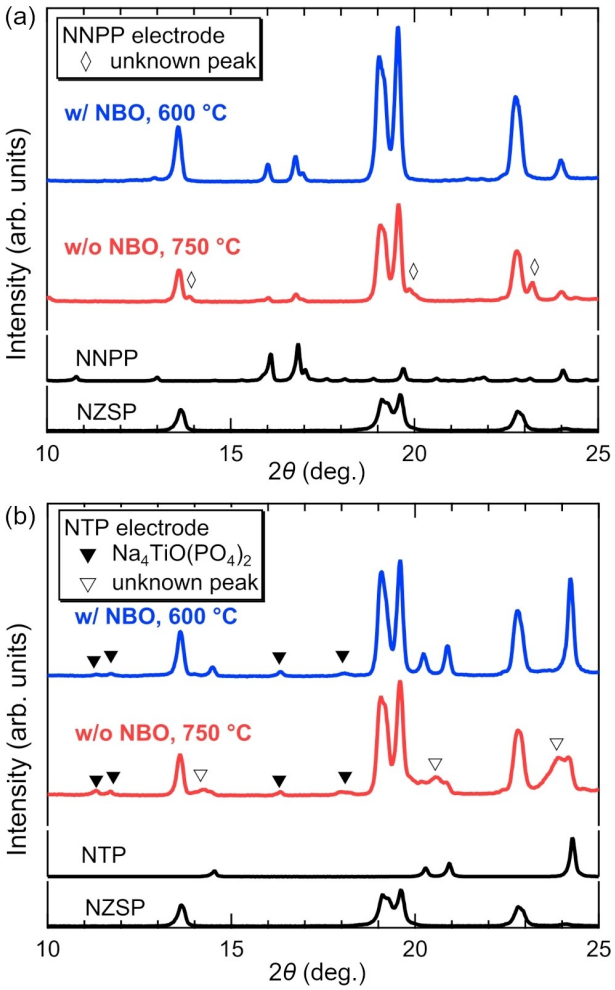

Figure 1. XRD patterns of a) the NNPP positive electrodes and b) the NTP negative electrodes in the NTP/NZSP/NNPP batteries fabricated at 600 °C with the NBO (blue) and at 750 °C without the NBO (red). The black patterns are powder XRD of the NZSP electrolyte, the NNPP active material, and the NTP active material.

because of their polyanionic framework.[15] Noted that an NTP half-cell using the liquid electrolyte exhibited a discharge capacity of 95 mAh g^{-1} in an operating voltage of 1.0–2.5 V vs. Na/Na^+ (Supporting Information Figure S2b), which was comparable to those of previous works, 90 mAh g^{-1}[13] and ~100 mAh g^{-1}.[16] However, a discharge capacity faded when the operating voltage was in 0–2.5 V vs. Na/Na^+, implying that solid electrolyte interfaces that were formed under low working voltage hindered the discharge. Thus, it is important to reveal the mechanism of the charge/discharge profiles of the NTP/NZSP/NNPP, especially in high operating voltage.

The NNPP active materials in the positive electrode were irreversible during the first charge/discharge process. Figure 2(c) shows ex situ XRD patterns of the positive electrode during the first charge/discharge depicted in Figure 2(b). In the pristine state, two distinct peaks were observed at ~16° (NNPP 011) and ~17° (NNPP 210). In the first charge process, the NNPP 011 peak and NNPP 210 peak were shifted to lower angle and to higher angle, respectively (pristine to 2.8 V), and then

Research Article
doi.org/10.1002/batt.202300075
Chemistry Europe
European Chemical Societies Publishing

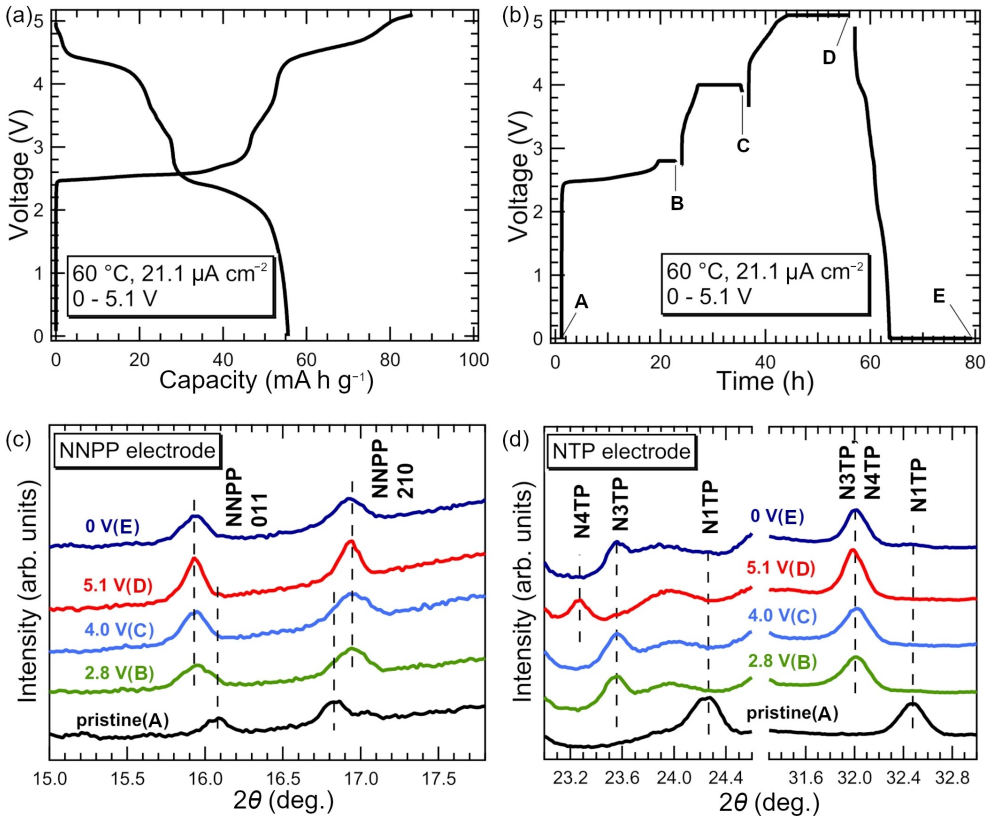

Figure 2. a) First cycle charge/discharge curves of the NTP/NZSP/NNPP batteries. b) First cycle charge/discharge curves of the NTP/NZSP/NNPP batteries during the ex situ XRD measurement. XRD was measured at pristine (A), 2.8 V (B), 4.0 V (C), 5.1 V (D), and 0 V (E). The *ex situ* XRD patterns of c) the NNPP electrode and d) the NTP electrode during the first cycle charge/discharge process. N1TP, N3TP, and N4TP in Figure (d) stand for $NaTi_2(PO_4)_3$, $Na_3Ti_2(PO_4)_3$, and $Na_4Ti_2(PO_4)_3$, respectively.

both peaks were sharpened (2.8–5.1 V). This voltage-dependent change of the diffraction peaks was attributed to sodium-ion removal from the NNPP lattice,[12] meaning that the NNPP active materials were successfully desodiated during the first charge process. In the first discharge process, however, the peaks did not move back to the original positions, which was considered an irreversible change of the $[Ni_3P_2O_{13}]$ layers in NNPP.[12] Hence, the low coulombic efficiency of the NTP/NZSP/NNPP batteries was related to the crystal rearrangement of the NNPP active materials during the charge/discharge process. The discharge capacity of the batteries in the ex situ XRD measurement (Figure 2b) was relatively low compared with that of the batteries in Figure 2(a). This variance of the capacity seemed to be a consequence of the decomposition of the NZSP electrolyte by maintaining a high voltage during the ex situ XRD, as we discuss later.

The voltage-dependent change of crystal structures in the NTP electrode implies that the characteristic three-stage charge/discharge behavior resulted from redox reactions of the NTP electrode. In the first charge stage (pristine to 2.8 V), $NaTi_2(PO_4)_3$ converted to $Na_3Ti_2(PO_4)_3$, for which the redox potential is 2.1 V vs. Na/Na^+,[13] causing the positive electrode potential to be ~4.9 V vs. Na/Na^+, which was corroborated by the peak shift of NNPP shown in Figure 2(c) and previous works.[12,14] In the second charge stage (2.8–4.0 V), the $Na_3Ti_2(PO_4)_3$ peaks remained, which means a species other than $Na_3Ti_2(PO_4)_3$ contributed to the battery reaction. A candidate of this reaction source is the $Na_4TiO(PO_4)_2$ impurity, which was observed by XRD (Figure 1) and is known to have a redox potential of 1.0–1.5 V vs. Na/Na^+,[17] which is in good agreement with the obtained battery voltage (2.8–4.0 V) because the positive electrode potential was estimated to be approximately 5 V vs. Na/Na^+. The $Na_4TiO(PO_4)_2$ impurity peaks were not detected in the ex situ XRD measurement because of intense background signals from the bag that was used to protect the battery from degradation (Supporting Figure S3). In the third charge stage (4.0–5.1 V), $Na_3Ti_2(PO_4)_3$ was converted to $Na_4Ti_2(PO_4)_3$, for which the redox potential is 0.4 V vs. Na/Na^+.[13] In the discharge process, $Na_4Ti_2(PO_4)_3$ was converted to a mixture of a substantial amount of $Na_3Ti_2(PO_4)_3$ and a tiny amount of $NaTi_2(PO_4)_3$, which can be explained by the large irreversibility of the positive electrode shown in Figure 2(c).

The NBO sintering aid suppressed oxidative decomposition of the NZSP electrolyte reasonably well under high operating potential. In a previous study,[18] first-principle calculations predict that NZSP oxidatively decomposes into $ZrSiO_4$, O_2, $NaZr_2(PO_4)_3$, and SiO_2 above 3.64 V vs. Na/Na^+, which means that NZSP is unstable against the redox potential of NNPP, approximately 5.0 V vs. Na/Na^+. Contrary to the theoretical calculations, however, most experimental reports claimed that

Research Article
doi.org/10.1002/batt.202300075
Chemistry Europe
European Chemical Societies Publishing

NZSP was stable up to at least 5.0 V vs. Na/Na^+,[19–24] whereas only a few reports pointed out that Mg-doped NZSP was oxidized at approximately 4.5 V[25] or 4.6 V vs. Na/Na^+.[26] This large discrepancy in the electrochemical stability comes from the sample design, as Han et al. pointed out.[27] In this study, the electrochemical stability of the NZSP electrolyte was carefully evaluated by measuring the linear sweep voltammetry or cyclic voltammetry of the NZSP + acetylene black (AB) electrode composite, which ensured sufficiently large reaction surface areas (Figure 3). Figure 3 shows that the NZSP electrolyte without the NBO was gradually oxidized above 3.0 V vs. Na/Na^+, followed by drastic oxidation at approximately 3.8 V vs. Na/Na^+, which was comparable with the theoretical prediction. It should be noted that this low electrochemical stability was not affected by high-temperature sintering because NZSP was stable up to at least 900 °C (Supporting Information Figure S4). Contrariwise, the NZSP electrolyte with the NBO was highly stable up to 4.0 V vs. Na/Na^+ and oxidized only gradually above that voltage, suggesting that the NBO protected the NZSP electrolyte from oxidative decomposition. The reduction/oxidation current was observed in the vicinity of 1.0 V vs. Na/Na^+, most likely corresponding to the irreversible reactions of the sodium ion with AB,[28] which might be somewhat associated with the large coulombic loss of the NTP/NZSP/NNPP batteries during the first cycle.

The cyclic performance of the NTP/NZSP/NNPP batteries was comparable with those of the previous works on NTP half-cells and NNPP half-cells using liquid electrolytes.[12,14,16] Figure 4(a) shows the cycling discharge capacities and coulombic efficiencies of the NTP/NZSP/NNPP battery in the first 10 cycles (see also Supporting Information Figure S5). After the large coulombic loss at the first cycle, mainly due to the irreversible change of the NNPP structure, the coulombic efficiency went up to 94%–97% in the following cycles with the capacity decay from 56 mAh g^{-1} to 40 mAh g^{-1} (the capacity retention of 71% after 10 cycles). This capacity retention was comparable with the predicted value from previous works, in which NTP half-cells with liquid electrolytes were reported to exhibit a capacity retention of approximately 90%,[16] and NNPP half-cells were reported to exhibit capacity retentions of 77%[12] and 90%–94%[14] after 10 cycles. However, the capacity retention of the NTP/NZSP/NNPP battery was rather low as compared with that of a $Na_3V_2(PO_4)_3$ symmetric AOSSSB fabricated by the same method, which had a capacity retention of 100% even after 99 cycles.[5]

One possible reason for the relatively low cycle stability of the NTP/NZSP/NNPP is the slight oxidative decomposition of the NZSP electrolyte under the high operating voltage. Figure 4(c) shows storage time-dependent impedance plots of the NTP/NZSP/NNPP battery stored at 2.8 V as shown in Figure 4(b). The cell voltage of 2.8 V corresponded to the end of the first

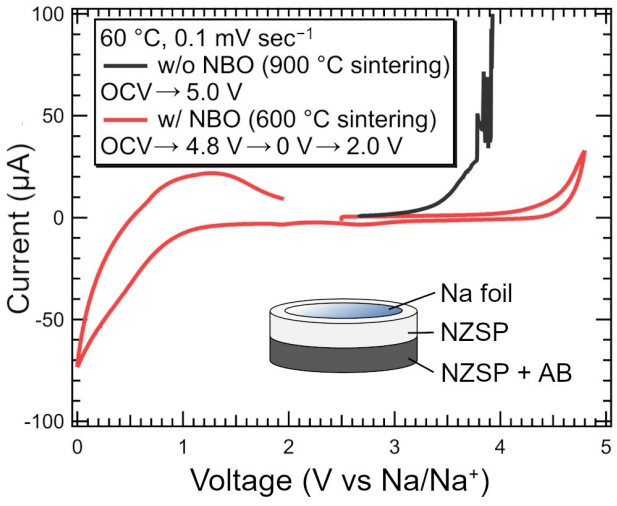

Figure 3. Linear sweep voltammogram (2.7–5.0 V) of the Na/NZSP/NZSP + AB fabricated at 900 °C without the NBO sintering aid (black) and cyclic voltammogram (0–4.8 V) of the Na/NZSP/NZSP + AB fabricated at 600 °C with the NBO (red). The inset is a schematic image of the sample.

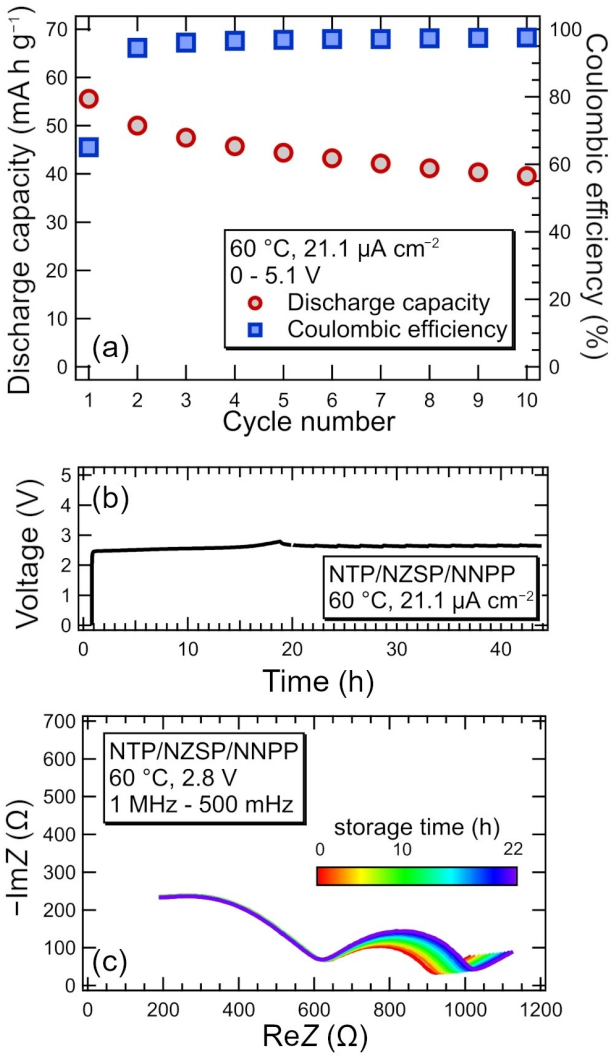

Figure 4. a) Cycling discharge capacity (red circles) and coulombic efficiency (blue squares) of the NTP/NZSP/NNPP battery. b) Time-dependent voltage curve of the NTP/NZSP/NNPP battery during the storage test. After the battery was charged to 2.8 V, electrochemical impedance spectroscopy was constantly measured for a period of 2 h. c) Storage time-dependent impedance plots of the NTP/NZSP/NNPP battery during the storage at 2.8 V shown in (b).

Research Article
doi.org/10.1002/batt.202300075
Chemistry Europe
European Chemical Societies Publishing

charge stage, where the negative electrode potential and the positive electrode potential were assumed to be ~2.1 V vs. Na/Na^+ and ~4.9 V vs. Na/Na^+, respectively, which was high enough to oxidize even the NBO containing NZSP electrolyte as shown in Figure 3. Each impedance plot presents three distinct components – the quarter-circle, the semi-circle, and the linear slope – corresponding to the electrolyte resistance, the charge-transfer resistance, and the sodium-ion transfer resistance, respectively (Supporting Information Figure S6).[29] The charge-transfer resistance increased with an increase in the storage time, suggesting that the NZSP electrolyte underwent oxidative decomposition because the oxidation products, such as $NaZr_2(PO_4)_3$, have a lower sodium-ionic conductivity in comparison with NZSP.[30,31] Zhang et al. also reported that Mg-doped NZSP with a liquid electrolyte was oxidatively decomposed under a high operating voltage, which led to the poor cycle performance.[26] Consequently, the high-voltage operation caused the oxidation of the NZSP electrolyte, leading to the low coulombic efficiency and the relatively low cycle stability, although the NBO somewhat protected the NZSP from the decomposition. Noted that no obvious intermediate layer was observed at the NZSP/NNPP interfaces even after cycling (Supporting Information Figure S7). Microscopic analysis using transmission electron microscope is needed for further discussion on the oxidation products.

Figure 5 summarizes the first discharge voltage and the first discharge capacity of state-of-the-art AOSSSBs. To the knowledge of the authors, the NTP/NZSP/NNPP batteries in this study present the highest discharge voltage, with an average of 3.1 V in the range of 0–5.1 V, among all AOSSSBs, whereas the capacity is relatively low in comparison with those of other AOSSSBs, which is linked to the low capacity of the NNPP active material. Recently, high-capacity and high-potential positive active materials and high-capacity and low-potential negative active materials have been intensively studied. A $Na_{2/3}Fe_{1/2}Mn_{1/2}O_2$ positive active material has exhibited a discharge capacity of 166 mAh g^{-1} in a redox potential of 2.0–4.2 V vs. Na/Na^+,[32] whereas a $Na_3V_2(PO_4)_2F_3$ positive active material has shown a redox potential of 3.95 V vs. Na/Na^+ and a discharge capacity of 120 mAh g^{-1}.[33] A $Na_2Ti_3O_7$ negative active material has been reversibly sodiated/desodiated with a capacity of 200 mAh g^{-1} at a redox potential of 0.3 V vs. Na/Na^+.[28] Therefore, fabrication of AOSSSBs with higher voltage and capacity should be possible by applying our technique to a wide range of active materials.

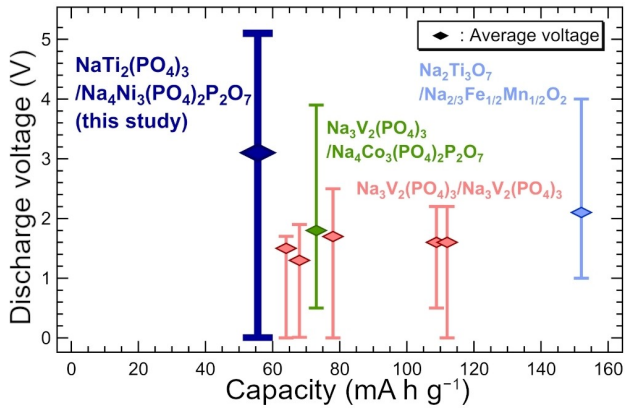

Figure 5. Comparison of state-of-the-art AOSSSBs ($Na_3V_2(PO_4)_3$/$Na_3Zr_2(SiO_4)_2(PO_4)$-related electrolyte/$Na_3V_2(PO_4)_3$ (red),[5–8] $Na_3V_2(PO_4)_3$/$Na_3Zr_2(SiO_4)_2(PO_4)$/$Na_4Co_3(PO_4)_2(P_2O_7)$ (green),[9] and $Na_2Ti_3O_7$/β''-Al_2O_3/$Na_{2/3}Fe_{1/2}Mn_{1/2}O_2$ (blue)[10]) and the NTP/NZSP/NNPP batteries (purple). The bars and the diamond symbols are the operating discharge voltage ranges and average discharge voltages, respectively. The discharge capacity is normalized by each cathode composite weight.

Conclusions

In this study, we successfully fabricated AOSSSBs with an operating voltage of 3.1 V, which are composed of the NTP negative active material, the NNPP positive active material, and the NZSP solid electrolyte, by using a flux-assisted low-temperature fabrication technique. The charge/discharge curves show a characteristic three-stage profile, which originates from the two-step redox reaction of the NTP and the redox reaction of the $Na_4TiO(PO_4)_2$ impurity. The NBO sintering aid helps the battery not only to be densified at the low temperature but also to be more stable even under a high voltage, realizing a capacity retention of 71% after 10 cycles under a high operating voltage (0–5.1 V).

Experimental

Fabrication of the NTP/NZSP/NNPP batteries

The NTP/NZSP/NNPP batteries were fabricated using a flux-assisted low-temperature fabrication technique.[5] As starting materials, an NZSP electrolyte composite was prepared by mixing NZSP powder (99.9%, Toshima Manufacturing Co., Ltd.) and NBO powder (≥ 99.5%, FUJIFILM Wako Pure Chemical Co.) with a weight ratio of 90:10. An NTP negative electrode composite was obtained by mixing NTP powder (99.9%, Toshima Manufacturing Co., Ltd.), the NZSP powder, AB (Denka Co., Ltd.), and the NBO powder with a weight ratio of 28:66:5:1. Similarly, an NNPP positive electrode composite was obtained in the same way as the NTP composite except for using NNPP powder (99.9%, Toshima Manufacturing Co., Ltd.). Initially, the NZSP electrolyte composite (83.3 mg) was placed in a graphite die with a diameter of 10 mm and pressed under a uniaxial pressure of 366 MPa to make an NZSP electrolyte layer. Next, the NTP electrode composite (10.8 mg) and the NNPP electrode composite (24.0 mg) were mounted on each side of the NZSP electrolyte layer and pressed under a uniaxial pressure of 146 MPa. Then, graphite sheets were placed on both sides of the pressed NTP/NZSP/NNPP, followed by re-pressing under a uniaxial pressure of 146 MPa. Finally, the pressed sample was sintered at 600 °C for 10 min under a uniaxial pressure of 102 MPa using commercial spark-plasma sintering (SPS) equipment (SPS-511ET, Sumitomo Coal Mining Co., Ltd.). For comparison, NTP/NZSP/NNPP batteries without the NBO sintering aid were also fabricated at 750 °C in a similar manner as detailed above. The above processes were carried out in a dry room with a dew point of less than −65 °C.

Fabrication of Na/NZSP/NZSP + AB samples

Na/NZSP/NZSP + AB samples were fabricated by a two-step process: fabrication of an NZSP/NZSP + AB pellet and the subsequent attachment of a Na foil (Sigma-Aldrich, 99.95%) onto the pellet. Firstly, an NZSP + AB electrode composite was prepared by mixing the NZSP electrolyte composite and the AB powder with a weight ratio of 82:18. Secondly, the NZSP electrolyte composite (166.7 mg) was placed in the graphite die and pressed under a uniaxial pressure of 366 MPa, followed by mounting the NZSP + AB electrode composite (102.1 mg) onto one side of the NZSP electrolyte layer and re-pressing the sample under a uniaxial pressure of 146 MPa. Thirdly, the pressed sample was sintered at 600 °C for 10 min under a uniaxial pressure of 102 MPa using the SPS equipment. Finally, the Na foil was attached onto the other side of the NZSP electrolyte layer, and then the obtained Na/NZSP/NZSP + AB samples were enclosed by bags in an Ar-filled glove box. Similarly, Na/NZSP/NZSP + AB batteries without the NBO sintering aid were also fabricated at 900 °C, which was high enough to fabricate robust batteries.

Fabrication of NNPP half-cell and NTP half-cell

Composite positive electrodes comprising 80 wt% active materials (NNPP or NTP), 11 wt% AB, and 9 wt% polyvinylidene difluoride dissolved in 1-methyl-2-pyrrolidone were pasted onto Al foil current collector, and then the electrodes was dried at 100 °C and uniaxially pressed. CR2032-type coin cells with the positive electrode, Na foil negative electrode, 1.0 M $NaPF_6$ dissolved in ethylene carbonate/diethyl carbonate liquid electrolyte, and a separator were assembled in the Ar-filled glove box.

Characterization

The NTP/NZSP/NNPP batteries with the NBO sintering aid enclosed by Ar-filled bags were charged/discharged in the voltage range of 0–5.1 V at an electrical current of 21.1 μA cm^{-2}. Electrochemical impedance spectroscopy (EIS) of the battery was carried out with an alternating current amplitude of 30 mV in a frequency range from 1 MHz to 500 mHz before and after charging the battery to 2.8 V with a relaxation period of 1 h. Afterwards, a storage time-dependent resistance of the batteries at 2.8 V was evaluated by measuring the EIS constantly for a period of 2 h. Linear sweep voltammetry was conducted on the Na/NZSP/NZSP + AB without the NBO by sweeping the sample voltage from the open-circuit voltage (OCV, 2.7 V) to 5.0 V with a scanning rate of 0.1 mV sec^{-1}. Likewise, cyclic voltammetry of the Na/NZSP/NZSP + AB with NBO was measured by sweeping the sample voltage from the OCV (2.5 V) to 4.8 V and then back to zero, followed by sweeping the voltage to 2.0 V with a scanning rate of 0.1 mV sec^{-1}. All above electrochemical characterizations were carried out by using a commercial charge/discharge system (VMP3, Biologic) at 60 °C. The NNPP half-cells (NTP half-cells) were charged/discharged in the voltage range of 1.5–5.1 V (1.0–2.5 V or 0–2.5 V) at an electrical current of C/20 under 25 °C.

XRD with a θ–2θ method using Cu K_α radiation was employed to evaluate the stability of the NTP negative electrode and the NNPP positive electrode in NTP/NZSP/NNPP batteries with and without NBO after fabrication. The battery voltage-dependent change of the crystal structures in the electrodes was evaluated by measuring *ex situ* XRD after charging the NTP/NZSP/NNPP batteries to 2.8 V, 4.0 V, and 5.1 V at a constant electrical current of 21.1 μA cm^{-2} and a subsequent constant-voltage holding under 60 °C. During the ex situ XRD, the batteries were covered by bags to protect the batteries from degradation. The cross-sectional morphology of the batteries was investigated by a scanning electron microscope (Quanta 250, FEI), where the acceleration voltage of the electron beam was set at 15.0 kV. The thermal behavior of NZSP was evaluated by thermogravimetric analyzer (EXSTAR6000, Seiko Instruments Inc.).

Acknowledgements

This paper is based on results obtained from a project, JPNP14004, commissioned by the New Energy and Industrial Technology Development Organization (NEDO).

Conflict of Interests

The authors declare no conflict of interest.

Data Availability Statement

The data that support the findings of this study are available from the corresponding author upon reasonable request.

Keywords: all-oxide batteries · NASICON · sintering aids · solid-state batteries · sodium batteries

[1] J. A. Jeevarajan, T. Joshi, M. Parhizi, T. Rauhala, D. Juarez-Robles, *ACS Energy Lett.* **2022**, *7*, 2725.
[2] C. Helbig, A. M. Bradshaw, L. Wietschel, A. Thorenz, A. Tuma, *J. Cleaner Prod.* **2018**, *172*, 274.
[3] A. Manthiram, X. Yu, S. Wang, *Nat. Rev. Mater.* **2017**, *2*, 16103.
[4] C. Vaalma, D. Buchholz, M. Weil, S. Passerini, *Nat. Rev. Mater.* **2018**, *3*, 18013.
[5] D. Kutsuzawa, T. Kobayashi, S. Komiya, *ACS Appl. Energ. Mater.* **2022**, *5*, 4025.
[6] Y. Noguchi, E. Kobayashi, L. S. Plashnitsa, S. Okada, J. Yamaki, *Electrochim. Acta* **2013**, *101*, 59.
[7] F. Lalère, J. B. Leriche, M. Courty, S. Boulineau, V. Viallet, C. Masquelier, V. Seznec, *J. Power Sources* **2014**, *247*, 975.
[8] Q. Ma, C. Tsai, X. Wei, M. Heggen, F. Tietz, J. T. S. Irvine, *J. Mater. Chem. A* **2019**, *7*, 7766.
[9] T. Kobayashi, F. Chen, V. Seznec, C. Masquelier, *J. Power Sources* **2020**, *450*, 227597.
[10] T. Wei, Y. Gong, X. Zhao, K. Huang, *Adv. Funct. Mater.* **2014**, *24*, 5380.
[11] H.-B. Sun, J.-Z. Guo, Y. Zhang, T. Wei, Y.-X. Zhou, L.-L. Zhang, X.-L. Wu, Y. Huang, W. Luo, *ACS Appl. Mater. Interfaces* **2019**, *11*, 24192.
[12] H. Zhang, I. Hasa, D. Buchholz, B. Qin, D. Geiger, S. Jeong, U. Kaiser, S. Passerini, *NPG Asia Mater.* **2017**, *9*, e370.
[13] P. Senguttuvan, G. Rousse, M. E. Arroyo y de Dompablo, H. Vezin, J.-M. Tarascon, M. R. Palacín, *J. Am. Chem. Soc.* **2013**, *135*, 3897.
[14] P. R. Kumar, H. B. Yahia, I. Belharouak, M. T. Sougrati, S. Passerini, R. Amin, R. Essehli, *J. Solid State Electrochem.* **2020**, *24*, 17.
[15] A. Gezović, M. J. Vujković, M. Milović, V. Grudić, R. Dominko, S. Mentus, *Energy Storage Mater.* **2021**, *37*, 243.
[16] J. Liang, K. Fan, Z. Wei, X. Gao, W. Song, J. Ma, *Mater. Res. Bull.* **2018**, *99*, 343.
[17] Q. Wang, K. S. Dai, Y. Xie, M. Shui, J. Shu, *Electrochim. Acta* **2021**, *381*, 138272.
[18] V. Lacivita, Y. Wang, S.-H. Bo, G. Ceder, *J. Mater. Chem. A* **2019**, *7*, 8144.
[19] J. Yang, H. L. Wan, Z. H. Zhang, G. Z. Liu, X. X. Xu, Y. S. Hu, X. Y. Yao, *Rare Met.* **2018**, *37*, 480.
[20] Y. Zhao, C. Wang, Y. Dai, H. Jin, *Nano Energy* **2021**, *88*, 106293.
[21] Y. Xing, Y. Li, C. Zhang, *Solid State Ionics* **2021**, *373*, 115811.

[22] Y. Lu, J. A. Alonso, Q. Yi, L. Lu, Z. L. Wang, C. Sun, *Adv. Energy Mater.* **2019**, *9*, 1901205.
[23] L. Shen, J. Yang, G. Liu, M. Avdeev, X. Yao, *Mater. Today Energy* **2021**, *20*, 100691.
[24] W. Zhou, Y. Li, S. Xin, J. B. Goodenough, *ACS Cent. Sci.* **2017**, *3*, 52.
[25] S. Song, H. M. Duong, A. M. Korsunsky, N. Hu, L. Lu, *Sci. Rep.* **2016**, *6*, 32330.
[26] Q. Zhang, Q. Zhou, Y. Lu, Y. Shao, Y. Qi, X. Qi, G. Zhong, Y. Yang, L. Chen, Y.-S. Hu, *Engineering* **2022**, *8*, 170.
[27] F. Han, Y. Zhu, X. He, Y. Mo, C. Wang, *Adv. Energy Mater.* **2016**, *6*, 1501590.
[28] P. Senguttuvan, G. Rousse, V. Seznec, J.-M. Tarascon, M. R. Palacín, *Chem. Mater.* **2011**, *23*, 4109.
[29] W. Zhang, D. A. Weber, H. Weigand, T. Arlt, I. Manke, D. Schröder, R. Koerver, T. Leichtweiss, P. Hartmann, W. G. Zeier, J. Janek, *ACS Appl. Mater. Interfaces* **2017**, *9*, 17835.
[30] J. B. Goodenough, H.-P. Hong, J. A. Kafalas, *Mater. Res. Bull.* **1976**, *11*, 203.
[31] K. D. Kreuer, H. Kohler, U. Warhus, H. Schulz, *Mater. Res. Bull.* **1986**, *21*, 149.
[32] K. Park, D. Han, H. Kim, W. Chang, B. Choi, B. Anass, S. Lee, *RSC Adv.* **2014**, *4*, 22798.
[33] R. A. Shakoor, D.-H. Seo, H. Kim, Y.-U. Park, J. Kim, S.-W. Kim, H. Gwon, S. Lee, K. Kang, *J. Mater. Chem.* **2012**, *22*, 20535.

Manuscript received: February 28, 2023
Revised manuscript received: April 21, 2023
Accepted manuscript online: May 7, 2023
Version of record online: May 22, 2023